

# Racemic Peptides from Amyloid $\beta$ and Amylin Form Rippled $\beta$ -Sheets Rather Than Pleated $\beta$ -Sheets

Amaruka Hazari,\*<sup>§</sup> Michael R. Sawaya,<sup>§</sup> Maria Sajimon, Niko Vlahakis, Jose Rodriguez, David Eisenberg, and Jevgenij A. Raskatov\*



Cite This: *J. Am. Chem. Soc.* 2023, 145, 25917–25926



Read Online

ACCESS |

Metrics & More

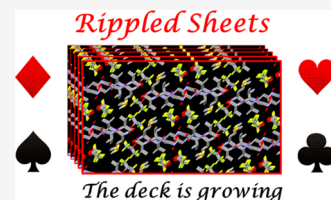


Article Recommendations



Supporting Information

**ABSTRACT:** The rippled  $\beta$ -sheet was theorized by Pauling and Corey in 1953 as a structural motif in which mirror image peptide strands assemble into hydrogen-bonded periodic arrays with strictly alternating chirality. Structural characterization of the rippled  $\beta$ -sheet was limited to biophysical methods until 2022 when atomic resolution structures of the motif were first obtained. The crystal structural foundation is restricted to four model tripeptides composed exclusively of aromatic residues. Here, we report five new rippled sheet crystal structures derived from amyloid  $\beta$  and amylin, the aggregating toxic peptides of Alzheimer's disease and type II diabetes, respectively. Despite the variation in peptide sequence composition, all five structures form antiparallel rippled  $\beta$ -sheets that extend, like a fibril, along the entire length of the crystalline needle. The long-range packing of the crystals, however, varies. In three of the crystals, the sheets pack face-to-face and exclude water, giving rise to cross- $\beta$  architectures grossly resembling the steric zipper motif of amyloid fibrils but differing in fundamental details. In the other two crystals, the solvent is encapsulated between the sheets, yielding fibril architectures capable of host–guest chemistry. Our study demonstrates that the formation of rippled  $\beta$ -sheets from aggregating racemic peptide mixtures in three-dimensional (3D) assemblies is a general phenomenon and provides a structural basis for targeting intrinsically disordered proteins.



## INTRODUCTION

The incorporation of D-amino acids into proteins and peptides is a versatile strategy that generates mixed chirality frameworks with unique structural and functional properties. Such frameworks have been employed to enhance protein activity,<sup>1–4</sup> modulate peptide aggregation,<sup>5–8</sup> and produce peptidic biomaterials with distinctive properties.<sup>9–14</sup> The development of new peptidic systems that contain both L- and D-amino acids has the potential to allow for systematic access to an unexplored structural space.

An example of a mixed chirality framework is the rippled  $\beta$ -sheet, which was first proposed as a theoretical concept by Pauling and Corey in 1953.<sup>15</sup> In a rippled  $\beta$ -sheet, D- and L-peptide strands are arrayed in a strictly alternating fashion, giving rise to a distinct backbone topography. Although the rippled  $\beta$ -sheet was conceptualized 70 years ago, a critical mass of experiments in support of its existence has only recently emerged.<sup>5,9–13,16–24</sup> The history of the field up to 2021 was recently reviewed by Raskatov, Schneider, and Nilsson.<sup>25</sup>

In a previous work, we demonstrated that racemic mixtures of 40- and 42-residue amyloid- $\beta$  peptides (D,L-A $\beta$ 40 and D,L-A $\beta$ 42) form fibrils with accelerated kinetics and enhanced stability relative to their homochiral counterparts (L-A $\beta$ 40 and L-A $\beta$ 42).<sup>5,21</sup> This effect, termed chiral inactivation, protects neuronal model systems from A $\beta$  neurotoxicity. Further studies, in collaboration with Tycko and co-workers, provided insight into the structural basis for chiral inactivation.<sup>24</sup> We showed that rather than the parallel  $\beta$ -sheets formed in

naturally observed L-A $\beta$  fibrils, the racemic counterparts form antiparallel  $\beta$ -sheets in which D- and L-A $\beta$  molecules alternate along the direction of fibril growth, forming a rippled  $\beta$ -sheet. We subsequently obtained the first atomic resolution structures from a series of model tripeptide systems, providing unambiguous structural evidence for the rippled  $\beta$ -sheet.<sup>22,23</sup>

Here, we report results from atomic-resolution crystallographic studies on racemic mixtures of peptides from segments of the disease-forming proteins A $\beta$  and amylin (Supporting Information (SI), Table S1). Our motivation for pursuing this work was threefold. Given that only a handful of atomic-resolution structures of rippled sheets have been obtained and are limited to tripeptide sequences composed of aromatic residues, our first objective was to expand the crystallographic foundation to include sequences of greater length and complexity. Structural evidence for the formation of rippled sheets from more complex racemic peptides such as MAX1,<sup>9,10</sup> KFE8,<sup>11,13</sup> Ac-KLVFFAE-NH<sub>2</sub>,<sup>13</sup> and YTIAALLSPYS<sup>26</sup> has only been obtained by indirect, biophysical methods.

Second, our results in support of rippled sheets in D,L-A $\beta$ 40 fibrils suggest that rippled sheet formation is a generic property

Received: October 20, 2023

Revised: November 2, 2023

Accepted: November 3, 2023

Published: November 16, 2023



ACS Publications

© 2023 American Chemical Society

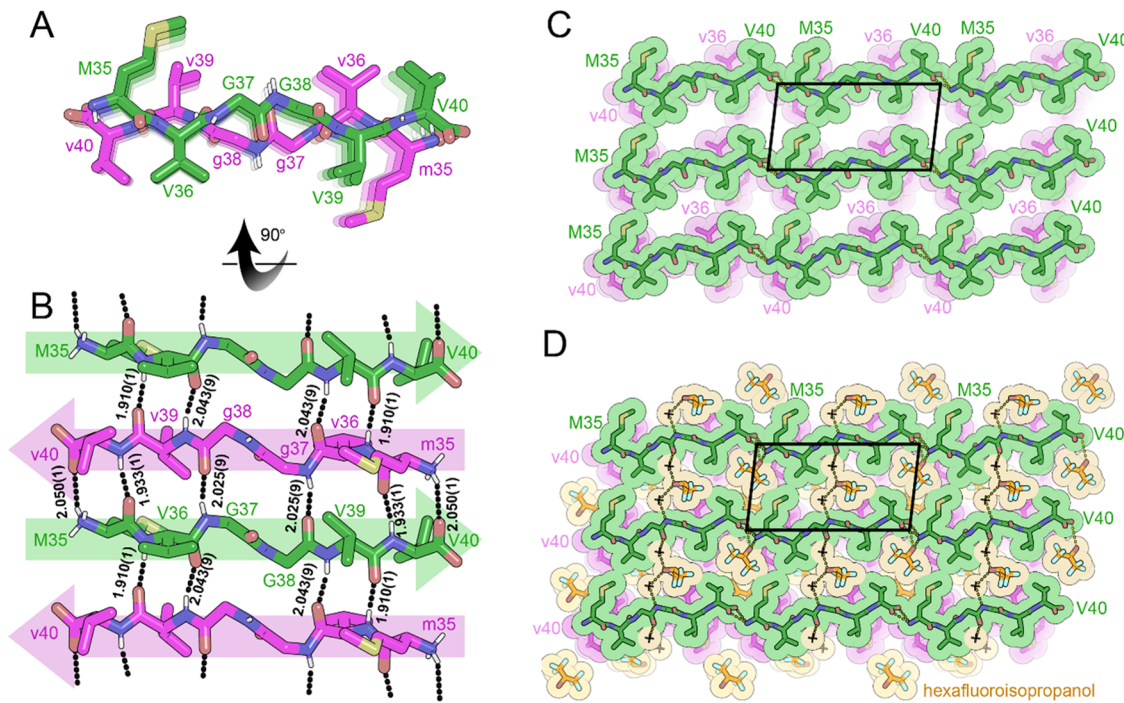


**Figure 1.** X-ray crystal structure of the rippled  $\beta$ -sheet formed by MVGGVV hexapeptide and its enantiomer mvggvv, MVGGVV:mvggvv in a mixture of hexafluoroisopropanol (HFIP) and water. (A) A view down the sheet hydrogen-bonding direction reveals rippling of the sheet. L-peptides are shown in green; D-peptides are shown in purple. (B) A view of the sheet face revealing the antiparallel in-register alignment of strands. Backbone H-bond distances ( $H \cdots O$ ) are reported in angstrom units [ $\text{\AA}$ ]. All backbone amides are involved in stabilizing the rippled sheet except for the amide linkage between G37 and G38, which is rotated out of the plane of the rippled sheet. (C) Crystal packing viewed along the H-bonding direction reveals gaps between sheet faces; contacts are sparse. The unit cell is outlined in black. (D) Gaps between sheet faces are filled by HFIP and water molecules (orange color). The integral role of solvent in maintaining the sheet interface explains why evaporation of HFIP causes crystal dissolution within seconds.

of racemic mixtures of amyloid-like peptide assemblies. We wished to test this hypothesis further by crystallizing short fragments from peptides that form amyloid-like fibrils. Furthermore, the choice of these peptide systems would allow us to make comparisons with solution-state nuclear magnetic resonance (NMR) studies<sup>27</sup> on model peptides from  $\text{A}\beta$ , which show a clear preference for homochiral assembly over heterochiral assembly.

A third objective was to compare the atomic resolution structures of racemic crystals to those of existing enantiopure crystals. Both crystal types assemble on a cross- $\beta$  scaffold, where individual  $\beta$ -strands orient perpendicular to the length of the crystalline needle and stack in  $\beta$ -sheets that run the entire length of the needle. Crystals of enantiopure amyloidogenic peptides have typically revealed tight mating between adjacent  $\beta$ -sheet surfaces, excluding water from their interface. This structural motif, called a “steric-zipper,” lends amyloid fibrils their extraordinary stability.<sup>28</sup> Are rippled sheets capable of mating in an analogous fashion, or will a different structural space emerge?

To address these objectives, we selected four distinct peptide segments from  $\text{A}\beta$  and amylin, which varied in hydrophobicity, charge, and sequence length. All four sequences formed extended, antiparallel rippled  $\beta$ -sheets. Our findings demonstrate a clear preference for heterochiral rippled  $\beta$ -sheets over homochiral pleated  $\beta$ -sheets upon crystallization and suggest that the tendency for racemic peptides to form rippled  $\beta$ -sheets in three-dimensional systems is much greater than previously thought.

## RESULTS

Our previous work identified the hydrophobic, aromatic residues Phe, Tyr, and Trp as ripple-genic.<sup>22,23</sup> To determine whether sequences composed predominantly of nonaromatic, hydrophobic residues could form rippled sheets, we selected the MVGGVV segment from the C-terminus of  $\text{A}\beta$  ( $\text{A}\beta_{35-40}$ ). A racemic mixture of MVGGVV and mvggvv was crystallized from a solution of hexafluoroisopropanol (HFIP) in water, yielding needles of antiparallel rippled  $\beta$ -sheet layers as determined by X-ray crystallography (Figure 1A,B). The rippled interface was partially interrupted at the G37–G38 junction. As observed in the previously reported tripeptide structures, the individual tripeptides stack in the H-bonding dimension, forming extended antiparallel rippled  $\beta$ -sheet layers, in which mirror image peptide strands are arranged in a strictly alternating fashion. Each L-hexapeptide (Figure 1B, green) is sandwiched between two D-hexapeptides (Figure 1B, purple), and each D-hexapeptide is sandwiched between two L-hexapeptides in a periodic fashion within the individual  $\beta$ -sheets, with H-bond distances ranging from 1.910(1) to 2.050(1)  $\text{\AA}$ . Each hexapeptide has six H-bonds to one of its two direct neighbors in the layer (i.e., “tight dimer”) and four H-bonds to the other (i.e., “loose dimer”) (Figure 1B).

The torsional angles for glycine residues G37 and G38 are measured as  $\varphi = -69.04$  and  $\psi = 151.8$  and  $\varphi = -74.8$  and  $\psi = 168.6$ , respectively, for the L-hexapeptide and  $\varphi = 69.0$  and  $\psi = -151.8$  and  $\varphi = 74.8$  and  $-169.6$ , respectively, for the inversion-related D-hexapeptide. The G37 and G38  $\varphi$  angles are considerably smaller than those found in crystals of enantiomerically pure MVGGVV (see SI, Table S2), resulting

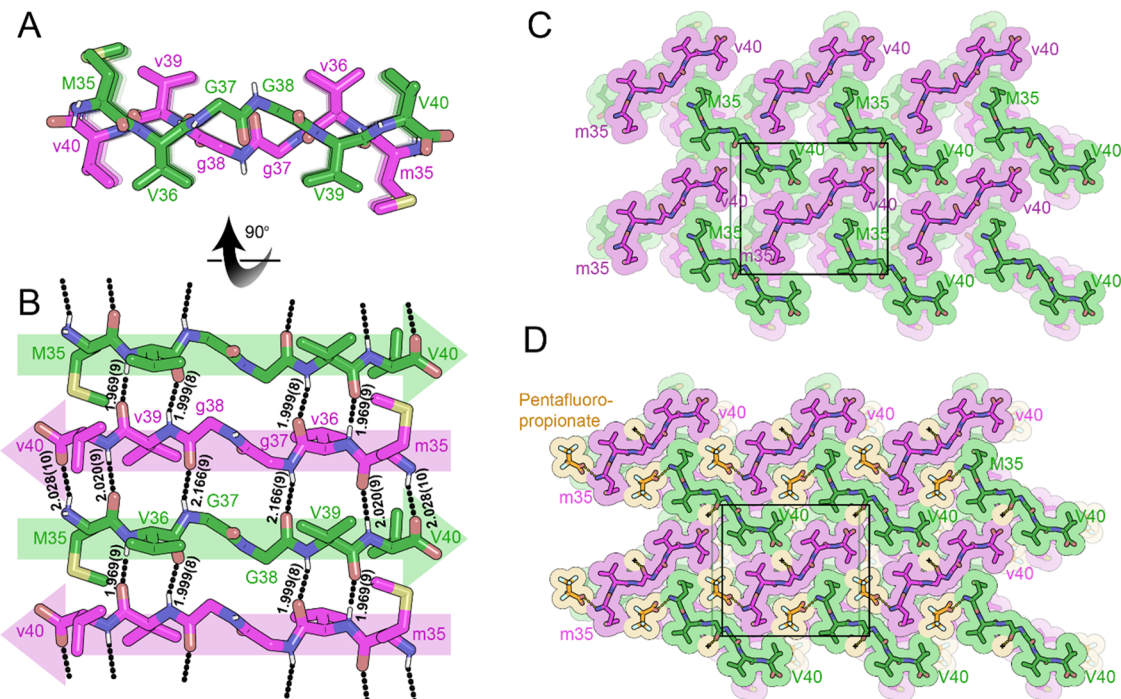


**Figure 2.** X-ray crystal structure of the rippled  $\beta$ -sheet formed by MVGGVV hexapeptide and its enantiomer mvggvv, MVGGVV:mvggvv in a mixture of pentafluoropropionic acid (PFPA) and water. (A) A view down the sheet hydrogen-bonding direction reveals rippling of the sheet. L-peptides are shown in green; D-peptides are shown in purple. (B) A view of the sheet face revealing the antiparallel in-register alignment of strands. Backbone H-bond distances ( $H \cdots O$ ) are reported in angstrom units [ $\text{\AA}$ ]. All backbone amides are involved in stabilizing the rippled sheet except for the amide linkage between G37 and G38, which is rotated out of the plane of the rippled sheet. (C) Crystal packing viewed along the H-bonding direction reveals the rippled sheets pack face-to-edge rather than face-to-face. The unit cell is outlined. (D) Small gaps in packing are filled by PFPA and water molecules (orange color).

in an  $\sim 90$ -degree rotation of the G37–G38 peptide plane from its standard orientation in a  $\beta$ -sheet.<sup>28</sup> An additional consequence of this rotation is the positioning of the V36 and V39 side chains; in the rippled sheet, the side chains reside on the same face of the  $\beta$ -sheet, whereas in the pleated sheet, V36 resides on the opposite face of the  $\beta$ -sheet from V39.<sup>28</sup>

Unlike many amyloid-like structures<sup>28</sup> and the tripeptide rippled sheet structures that we reported in the past,<sup>22</sup> pairs of rippled antiparallel sheets do not form a tight dry interface; instead, the sheets form a cavity, which encapsulates the HFIP molecules (Figure 1C,D). Pairs of rippled sheets are also associated in the lateral direction through the formation of salt bridges between N- and C-termini (Figure 1C, dashed lines). As a result, an additional cavity, running parallel to the fibril axis, forms between the salt bridges and the side chains of terminal residues of the rippled sheets; HFIP molecules are also trapped in this cavity and are hydrogen bonded to the carboxylate and ammonium termini of the loose dimer. Formation of the three-dimensional crystallographic lattice appears to be contingent on the presence of HFIP molecules, as exposure to air leads to the dissolution of crystals after several minutes.

Given the presence of a cavity, we were curious as to whether other fluorinated solvents could be incorporated into the extended crystallographic lattice and how they would influence the long-range packing. A polymorph of MVGGVV:mvggvv was obtained by the crystallization of a racemic mixture from a solution of water and pentafluoropropionic acid (PFPA). The resulting needles contained periodic MVGGVV:mvggvv antiparallel rippled  $\beta$ -sheet layers, as determined crystallographically (Figure 2A,B).

The packing of the individual hexapeptides in the H-bonding direction closely resembles that observed in the MVGGVV:mvggvv HFIP structure, alternating between tight and loose dimers. H-bond distances range between 1.969(9) and 2.166(9)  $\text{\AA}$ . The torsional angles for the glycine residues G37 and G38 are measured as  $\varphi = -68.2$  and  $153.1^\circ$  and  $\varphi = -68.8^\circ$  and  $\psi = 169.0^\circ$ , respectively, for the L-peptide and  $\varphi = 68.1^\circ$  and  $\psi = -151.7^\circ$  and  $\varphi = 68.2^\circ$  and  $\psi = -169.0^\circ$ , respectively, for the D-peptide. As observed in the MVGGVV:mvggvv HFIP structure, the G37–G38 peptide plane is rotated  $\sim 90^\circ$  from its standard orientation in a  $\beta$ -sheet and the V36 and V39 side chains reside on the same face of the  $\beta$ -sheet.

While the structures of the rippled dimers of MVGGVV:mvggvv HFIP and PFPA display close resemblance to each other, the three-dimensional crystallographic lattices of the structures differ considerably (Figure 2C,D). In the PFPA structure, pairs of rippled antiparallel sheets do not pack in a face-to-face arrangement but rather pack face-to-edge. A water molecule connecting G37 of one strand to G38 on the strand of the opposite chirality, in the tight dimer, also interacts with the N-terminus of the dimer in the opposite orientation, connecting face to edge or edge to face dimers. PFPA molecules are trapped in the crystal lattice but are not found between the rippled sheets. Instead, the PFPA molecules bind to the N and C termini of the loose dimer. The variation in long-range packing between the MVGGVV:mvggvv polymorphs most likely arises from differing protonation states at the C-terminus; PFPA is strongly acidic and can protonate the C-terminus of the peptide, while HFIP is only mildly acidic and cannot protonate.

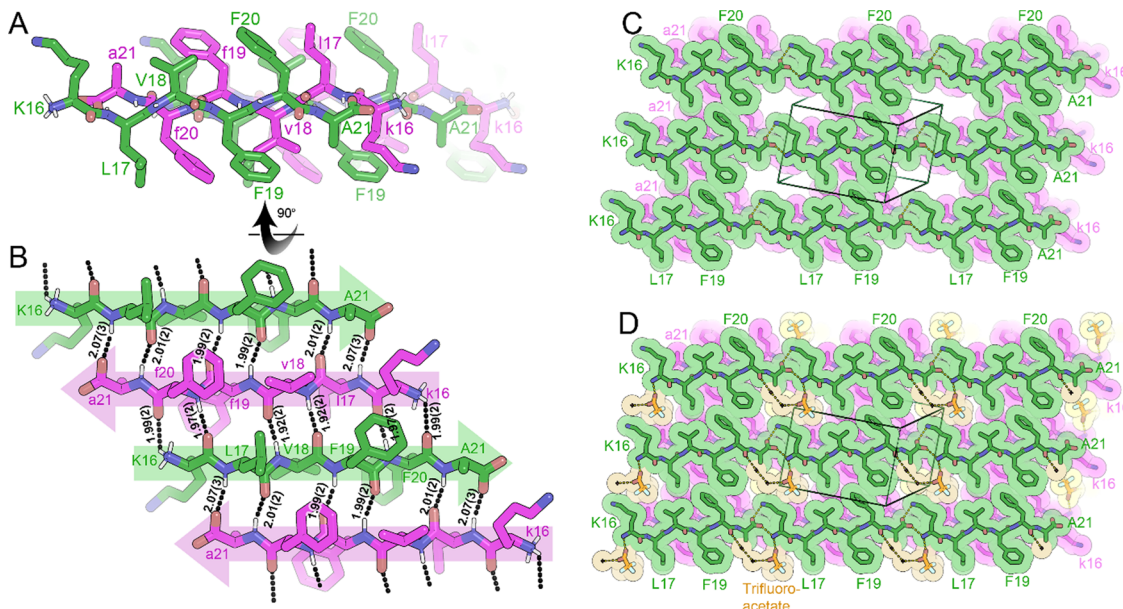


**Figure 3.** X-ray crystal structure of the rippled  $\beta$ -sheet formed by KLVFFA hexapeptide and its enantiomer klvffa, KLVFFA:klvffa in water and trifluoroacetate (TFA). (A) A view down the sheet hydrogen-bonding direction reveals rippling of the sheet. L-Peptides are shown in green; D-peptides are shown in purple. (B) A view of the sheet face revealing the antiparallel out-of-register alignment of strands. Lack of register is indicated by the sideways shift observed with each successive strand up and down the sheet. Backbone H-bond distances ( $H\cdots O$ ) are reported in angstrom units [ $\text{\AA}$ ]. All backbone amides are involved in stabilizing the rippled sheet. (C) Crystal packing viewed along the H-bonding direction reveals face-to-face packing via the hydrophobic side chains of L17, V18, F19, and F20. The unit cell is outlined. (D) Small gaps in packing are filled by TFA and water molecules (orange color).

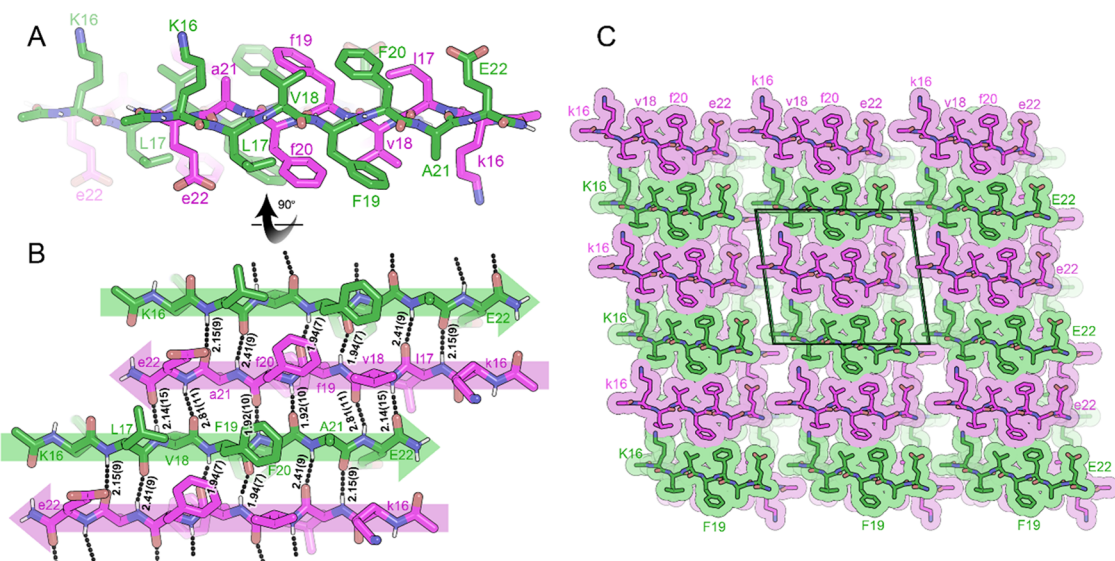


**Figure 4.** X-ray crystal structure of the rippled  $\beta$ -sheet formed by KLVFFAE hexapeptide and its enantiomer klvffae, KLVFFAE:klvffae in water and HFIP. (A) A view down the sheet hydrogen-bonding direction reveals rippling of the sheet. L-Peptides are shown in green; D-peptides are shown in purple. (B) A view of the sheet face revealing the antiparallel out-of-register alignment of strands. Lack of register is indicated by the sideways shift observed with each successive strand up and down the sheet. Backbone H-bond distances ( $H\cdots O$ ) are reported in angstrom units [ $\text{\AA}$ ]. All backbone amides are involved in stabilizing the rippled sheet. (C) Crystal packing viewed along the H-bonding direction reveals face-to-face packing via the hydrophobic side chains of L17, V18, F19, F20, and A21. The unit cell is outlined.

Encouraged by our ability to resolve the structures of these rippled  $\beta$ -sheets, we proceeded to explore the central hydrophobic region of  $\text{A}\beta$ . The KLVFFA segment ( $\text{A}\beta_{16-21}$ ) contains a charged residue at the N terminus as well as both aromatic and alkyl hydrophobic residues. A racemic mixture of KLVFFA and klvffa was crystallized from a solution of HFIP in water, yielding needles of antiparallel rippled  $\beta$ -sheets. The individual hexapeptides stack in the H-bonding

dimension, forming extended antiparallel rippled  $\beta$ -sheet layers (Figure 3A,B), similar to those observed in the structure of MVGGVV:mvggvv. In contrast to MVGGVV:mvggvv, the hexapeptide strands are tilted with respect to the “fibril” axis, resulting in an out-of-register sheet. As a consequence, only tight dimers are found in the KLVFFA:klvffa structure; each hexapeptide forms six hydrogen bonds to its two neighbors in the rippled sheet, with H-bond distances ranging from 1.92(2)

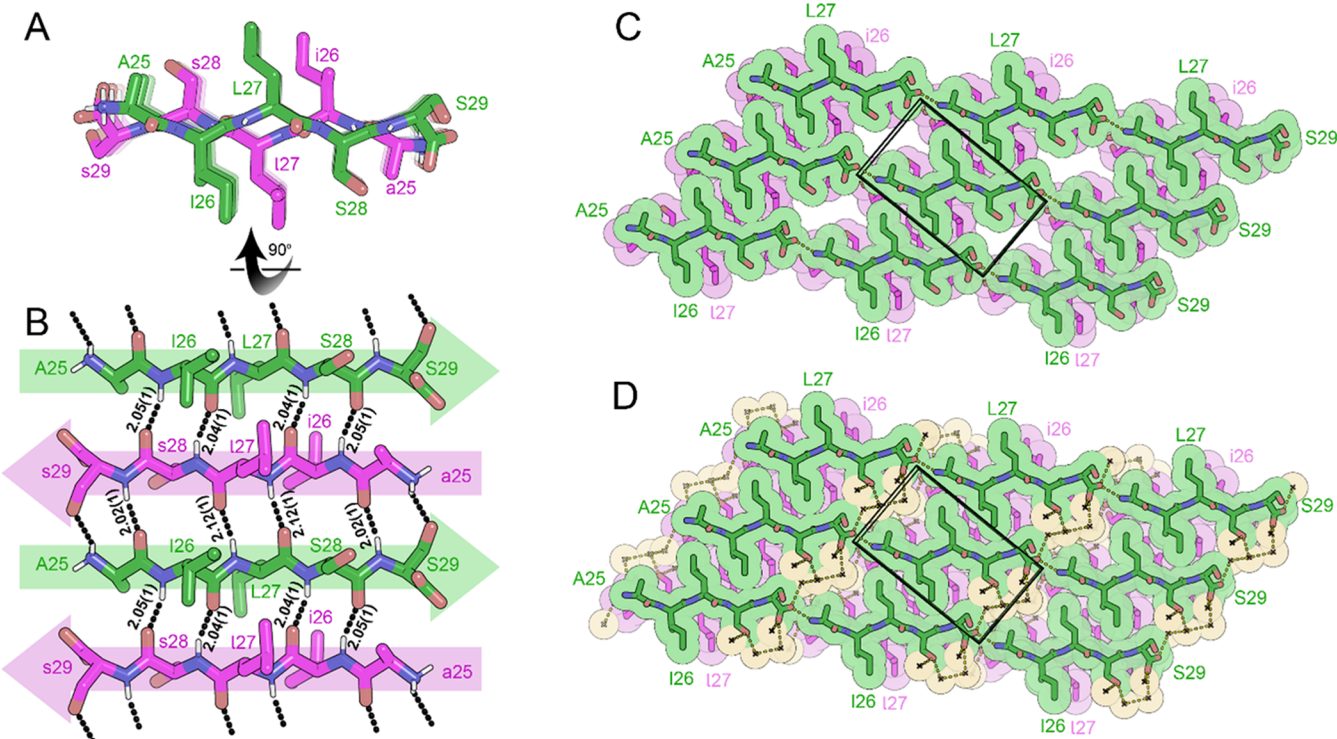


**Figure 5.** X-ray crystal structure of the rippled  $\beta$ -sheet formed by AILSS pentapeptide and its enantiomer ailss, AILSS:ailss in water and HFIP. (A) A view down the sheet hydrogen-bonding direction reveals rippling of the sheet. L-Peptides are shown in green; D-peptides are shown in purple. (B) A view of the sheet face revealing the antiparallel in-register alignment of strands. Backbone H-bond distances ( $H\cdots O$ ) are reported in angstrom units [ $\text{\AA}$ ]. All backbone amides are involved in stabilizing the rippled sheet. (C) Crystal packing viewed along the H-bonding direction reveals face-to-face packing via the hydrophobic side chains of I26 and L27. The unit cell is outlined. (D) Small gaps in packing are filled by water molecules (orange color).

to  $2.07(3)$   $\text{\AA}$ . In addition to the hydrogen bonds, CH-pi interactions are observed between the methylene protons of the K16 side chain and the aromatic ring of F20 on the strand of opposite chirality.

Tight packing between the hydrophobic side chains of L17, V18, F19, and F20 results in the formation of a dry interface between pairs of sheets (Figure 3C,D). CH-pi interactions are observed at the interface between the side chains of L17 and the aromatic rings of F19 and F20. In the lateral direction, the rippled dimers interact via salt bridges; the carboxylate terminus forms a salt bridge to the ammonium group of the K16 side chain as well as to the amino group of the N terminus of the neighboring dimer.

We subsequently examined the effect of adding an additional charge to the peptide sequence by expanding it C-terminally. The KLVFFAE segment of  $\text{A}\beta$  ( $\text{A}\beta$  16–22) contains polar, charged residues at both the N and C termini. Crystals of Ac-KLVFFAE-NH<sub>2</sub> and Ac-klvffae-NH<sub>2</sub> were grown from a solution of HFIP in water. X-ray and electron diffraction from the resulting needles extended to approximately 2.0  $\text{\AA}$  resolution, and a chemically reasonable model could be obtained by molecular replacement using an ideal  $\beta$ -strand as a search model. Difference density revealed the positions of the side chains. However, this atomic model produced unsatisfactory refinement statistics ( $R\text{-work } 0.465/R\text{-free } 0.490$ ). We attribute crystal disorder as the cause of the discrepancy between the atomic model and the diffraction data. The specific type of disorder is unclear, since twinning and translocation corrections produced no improvement in R-factors. Despite the limitations of the model, several key

features of the structure could be elucidated (Figure 4A,B). The individual heptapeptides stack in the H-bonding dimension, forming extended antiparallel rippled  $\beta$ -sheet layers with alternation of the L- and D-peptides. As observed with KLVFFA:klvffa, the heptapeptide strands are tilted with respect to the unit cell, forming an out-of-register sheet, with tight dimers between neighboring strands; H-bond distances range from  $1.92(10)$  to  $2.81(11)$   $\text{\AA}$ . Interestingly, the strand registration differs from KLVFFA:klvffa. In the KLVFFAE:klvffae rippled dimer, F19 stacks with F19 on the adjacent strand, whereas in KLVFFA:klvffa, V18 stacks with V18 on the adjacent strand.

Additionally, in the KLVFFAE:klvffae structure, the strands from adjacent sheets cross with an "X" pattern (Figure 4C), whereas in the KLVFFA:klvffa structure, all of the strands run parallel/antiparallel to the same, single axis. A study by Nilsson on the self-assembly of L- and D-KLVFFAE by Fourier-transform infrared (FTIR) and solid-state NMR proposes an in-register structure in which the antiparallel rippled sheets are precisely aligned.<sup>13</sup> Our structural model supports the proposed rippled antiparallel dimer but differs in that the individual dimers are offset with respect to each other within the sheet.

To explore whether the rippled sheet architecture is sufficiently robust to support sequences that include small polar residues, we chose to crystallize the pentapeptide sequence AILSS from amylin (residues 25–29). A racemic mixture of AILSS and ailss was crystallized from HFIP and water. Analysis of the needles by X-ray crystallography indicated the formation of antiparallel rippled sheets. Each

pentapeptide strand forms 4-H bonds to each of its neighbors with H-bond distances between the rippled dimers ranging from 2.018(11) to 2.123(10) Å (Figure 5A,B). The phi torsional angles for the two Ser residues differ considerably and are measured as  $\varphi = -145.03$  for S28 and  $\varphi = -77.53$  for S29. The S29 residue presumably adopts this conformation to hydrogen bond with the N-terminus of the adjacent strand. Rippled sheets mate face-to-face via a dry interface formed by packing of the hydrophobic side chains of I26 and Leu27 (Figure 5C,D). In contrast, the serine residues are surrounded by water molecules. Two water molecules connect S28 to the C terminus of a strand across the steric zipper.

## DISCUSSION

The assemblies formed by all five of our racemic peptides are unmistakably *heterochiral*; an observation that contrasts with the preference for *homochiral* assembly noted by Nowick's group in their study of model racemic  $\beta$ -sheet peptides derived from  $A\beta17-23$  and  $A\beta30-36$ .<sup>27</sup> A simplistic explanation for these disparate outcomes could be attributed to the different physical states of the two samples: crystalline in our studies and solution state in Nowick's studies. Wallach's rule predicts that homochiral packing is preferred in the solution state, whereas heterochiral packing is preferred in the crystalline state because it leads to denser solids.<sup>29</sup> Hence, crystal packing forces could have influenced our samples to form rippled sheets rather than conventional, homochiral pleated sheets, as observed in Nowick's studies. It is our view, however, that the force behind Wallach's rule (i.e., exclusion of solvent) is only a subset of the forces at play. Studies by Dunitz and Gavezzotti on chiral and racemic proteogenic amino acids illuminated violations of Wallach's rule; the most striking difference in density was observed for glutamine where the L-glutamine crystal was 11.8% more dense than the racemate.<sup>30</sup> Moreover, crystallization does not guarantee that a racemic peptide will assemble in a rippled sheet; a mixture of L-GSTSTA and D-gststa cocrystallized in adjacent assemblies of pure L- and pure D-pleated  $\beta$ -sheets.<sup>31</sup> It seems likely that the rippled  $\beta$ -sheet architecture observed here results from a compromise of several forces in addition to the exclusion of solvent, such as hydrogen-bonding, electrostatic complementation, and relief of torsional stress. Furthermore, the sequence of a peptide influences the balance of these forces and contributes to whether its racemic mixture ultimately forms a homochiral or heterochiral assembly.

It is important, however, to draw a clear distinction between the two-dimensional phenomenon of  $\beta$ -sheet assembly, defined by Pauling and Corey, and the three-dimensional phenomenon of crystallization, which drives the long-range packing of the individual sheets. It is also important to note that crystallization does not necessarily capture the most thermodynamically stable system, resulting from the assembly of strands in two dimensions. For example, at the dimer level, solution-state studies of constrained geometry peptide sequences have shown that pleated sheet formation is favored over rippled sheet formation. Liu and Gellman<sup>32</sup> showed that peptides designed to form two stranded  $\beta$ -hairpins, composed of half L and half D residues, did not exhibit heterochiral stand pairing when studied in solution. Similar observations were made by Nowick and co-workers from solution-state NMR studies conducted on both cyclic  $\beta$ -sheet peptides derived from  $A\beta17-23$  and  $A\beta30-36$ <sup>27</sup> and hydrophobic  $\beta$ -turn peptide mimics,<sup>33</sup> respectively.

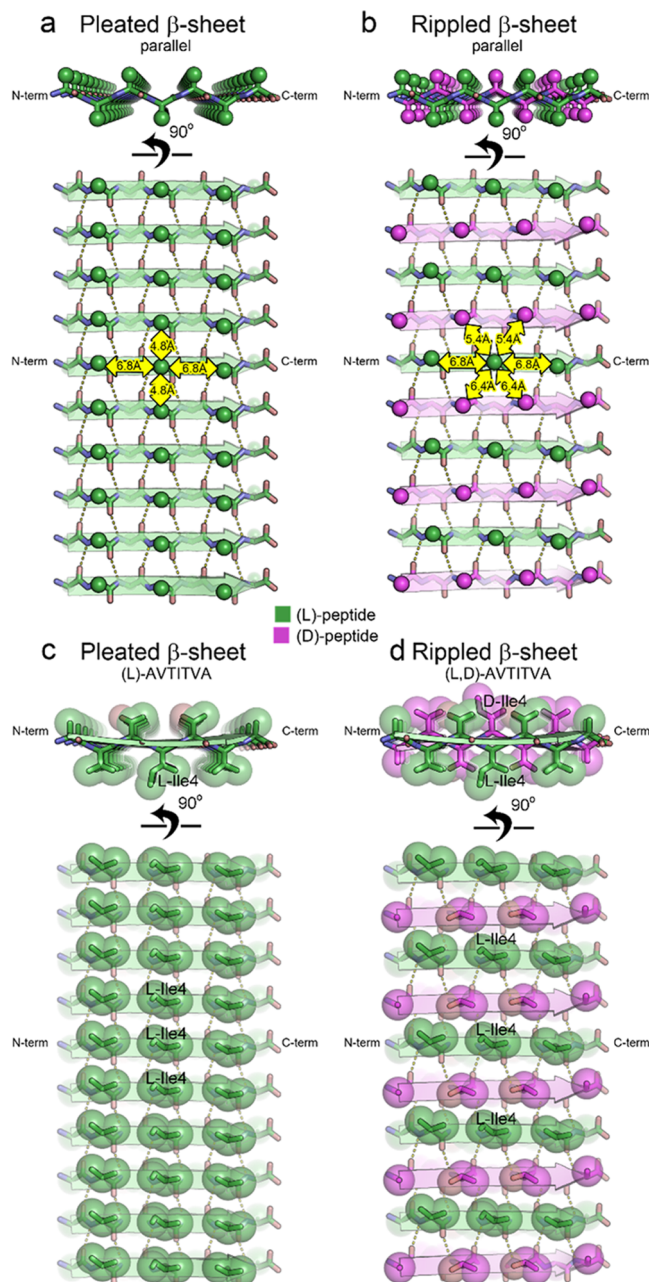


**Figure 6.** Pleated and rippled sheets exhibit distinct spatial arrangements of side chains. Sequences in C and D are added geometrically for illustrative purposes. (A) Pleated sheets characteristically arrange side chains (represented as spheres) 4.8 Å apart along the hydrogen-bonding direction (vertical yellow arrow) and 6.8 Å apart along the strand direction (horizontal yellow arrow). (B) Rippled sheets exhibit a wider, more isotropically spaced arrangement of side chains ranging from 5.4 to 6.8 Å separation. (C) The narrow spacing (4.8 Å) of side chains in pleated sheets creates the opportunity of forming stabilizing ladders of aliphatic, aromatic, or polar residues (esp. Asn and Gln) because side chains are close enough to form favorable van der Waals contacts or hydrogen bonds. On the other hand, the narrow spacing creates repulsion when neighboring side chains carry the same charge. (D) The wider, more isotropic spacing of rippled sheets eliminates the possibility of forming stabilizing ladders but relieves the repulsion when neighboring side chains carry the same charge.

The crystal structures described here provide an opportunity to discover whether rippled  $\beta$ -sheets are capable of packing

## Sheet-Sheet Interface Properties

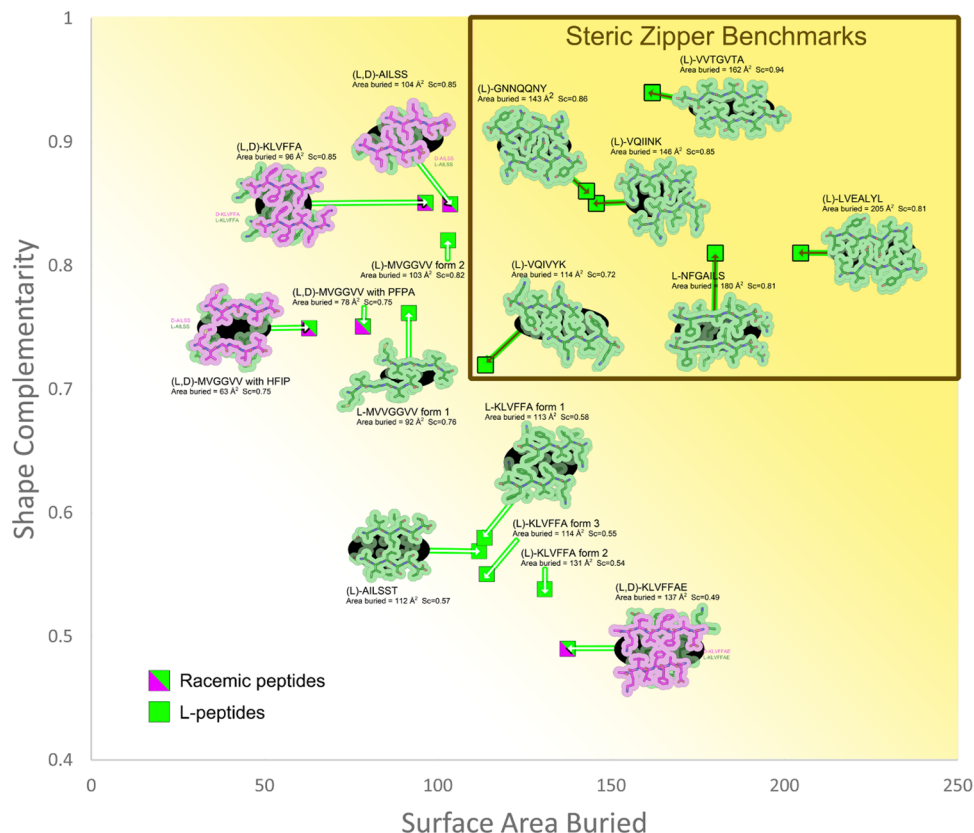


**Figure 7.** Comparison of crystallographic  $\beta$ -sheet interfaces of pleated versus rippled geometry. The strongest pleated sheet–sheet interfaces exhibit large areas of surface buried (right side of the graph) and fit together with high complementarity to exclude water (top side of the graph). Six benchmark steric zippers, known to drive (L)-proteins into amyloid fibrils, occupy the upper right corner of the graph. The zippers are viewed down the “fibril” axis. The interface between sheets is highlighted in black. The tightest zippers are those that show the least amount of black in their interface. Rippled sheet interfaces of (L,D)-AILSS and (L,D)-KLVFFA are near the steric zipper benchmark, having slightly lower buried surface area but good shape complementarity. Crystal structures of enantiopure (L)-AILSS and (L)-KLVFFA pleated sheets are shown for comparison to the corresponding rippled sheet interfaces. The pleated sheet interfaces for these sequences are also outside the benchmark region. This result suggests that rippled sheet interfaces fall outside the benchmark region due to low self-complementarity of the sequences rather than an inherent deficiency of rippled sheets to mate tightly.

together tightly and extensively enough to exclude solvent from their interface, as do the corresponding L-peptides in amyloid fibrils. Pleated and rippled sheets exhibit distinct spatial arrangements of side chains (Figure 6). Pleated sheets arrange side chains 4.8 Å apart along the hydrogen-bonding direction and 6.8 Å apart along the strand direction, whereas rippled sheets exhibit a wider, more isotropically spaced arrangement of side chains ranging from 5.4 to 6.8 Å spacings. These different arrangements may influence the capacity and geometry with which rippled sheets mate together. For example, the altered side chain arrangement may influence the angle at which two sheets prefer to interact or the ability of the rippled sheet surface to conform to a neighboring sheet surface and exclude water to form a dry interface.

We found dry sheet-to-sheet interfaces in some, but not all, of our rippled sheet structures. The MVGGVV:mvgvv crystal, grown in HFIP solvent, actually includes solvent in the interface rather than excluding it (Figure 1C,D), indicating that the surface shape of this rippled sheet is not self-complementary. Indeed, when this same racemic pair of peptides was crystallized in a different solvent, PFPA, the rippled sheets avoided face-to-face contact altogether and instead packed face-to-edge (Figure 2C). The remaining three

sheet-to-sheet interfaces packed face-to-face and excluded solvent molecules: KLVFFA:klvffa (Figure 3C,D), KLVFFAE:klvfae (Figure 4C,D), and AILSS:ailss (Figure 5C,D). These observations indicate that the rippled sheet architecture presents no fundamental obstacle to forming dry interfaces and that the extent and dryness of such an interface depends strongly on the amino acid sequence, as it does for pleated sheets of L-peptides (see SI, Table S3).

Two quantitative measures of amyloid stability are the surface area buried ( $\text{\AA}^2$ ) at the interface between mating sheets and shape complementarity (Sc).<sup>34</sup> The rippled sheet interface AILSS:ailss exhibits the size and self-complementarity approaching that of classical steric zipper interfaces known to drive amyloid formation, such as GNNQQNY from Sup35,<sup>35</sup> VQIVYK and VQIINK from Tau,<sup>36,37</sup> LVEALYL from insulin,<sup>38</sup> and NFGAILS from amylin.<sup>39</sup> Crystal structures of the L-forms of these amyloidogenic peptides have been determined and revealed interfaces between  $\beta$ -pleated sheets that bury surface area in the range of 114–205  $\text{\AA}^2/\text{peptide}$  and fit together tightly, with shape complementarity, Sc,<sup>40</sup> in the range of 0.72–0.94 (see SI Table S3). If we consider these values as “steric-zipper benchmarks,” then the AILSS:ailss rippled sheet–sheet interface exhibits values approaching steric

# Sheet-Sheet Interface Properties

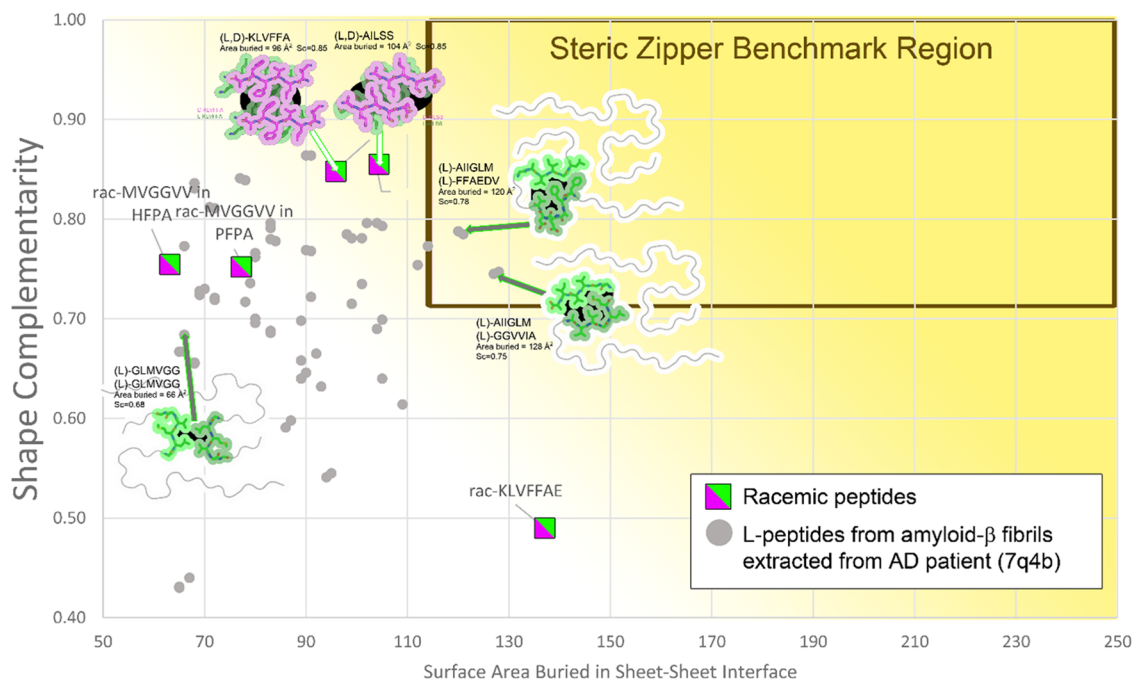


**Figure 8.** Comparison of  $\beta$ -sheet interfaces of rippled geometry (crystallographic) with those of pleated geometry found in amyloid- $\beta$  fibrils extracted from an Alzheimer's disease patient (PDB ID 7q4b). The strongest steric zippers exhibit large areas of surface buried (ABu) in the sheet–sheet interface and their sheets fit together with high complementarity (Sc) to exclude water (top right corner). Abu and Sc values for 104 pleated sheet interfaces, each 6-residues long, are plotted with gray dots. Two unique zippers from patient-extracted fibrils fall in the “steric zipper benchmark region.” The zippers are viewed down the “fibril” axis. The interface between sheets is highlighted in black. Crystal structures of ( $L,D$ )-AILSS and ( $L,D$ )-KLVFFA rippled sheets are shown for comparison to the pleated interfaces. The rippled sheet interfaces (green/magenta squares) fall outside the benchmark region, but most fall within the region of the segments found in patient-extracted fibrils.

zipper status, with a buried surface area of  $104 \text{ \AA}^2/\text{peptide}$  and Sc of 0.85. The three other peptide sequences in this study exhibited rippled sheet interfaces farther from the benchmark (Figure 7). The fact that the average size and fit of rippled sheet interfaces are lower than benchmark steric zippers may reflect the limited number of sequences probed here rather than an underlying geometric incapacity for rippled sheets to mate. We note that the sequences chosen for this study (MVGGVV, KLVFFA, and AILSS) produced relatively small, poor fitting pleated-sheet interfaces when crystallized as pure L-peptides (SI, Table S3). Exploration of other peptide sequences may reveal rippled sheet interfaces that rival the size and tight fit of steric zippers.

The steric zipper benchmarks in Figure 7 represent the strongest of the sheet–sheet interfaces, known to drive full-length proteins into amyloid fibrils. However, not every 6-residue sequence in an amyloid fibril meets this standard as the sheet–sheet interface size and fits vary (Figure 8). For example, we count 109 unique sheet–sheet interfaces of 6-residues long in brain-derived L-amyloid- $\beta$ (1:42) (PDB ID 7q4b). These have a median size of  $83 \text{ \AA}^2/\text{segment}$  and shape complementarity of 0.72. The five rippled sheet–sheet interfaces described here exhibit median values that slightly exceed these,  $96$  and  $0.75 \text{ \AA}^2$ , respectively. While these values fall below the benchmark values for L-peptide steric zippers, they do fall within the range observed in amyloid fibrils composed of full-length proteins. Our data suggest that the ability of rippled sheets to mate together is qualitatively similar to the mating of pleated sheets despite fundamental differences

in side chain arrangements on the respective sheet surfaces (Figure 6).

The rippled sheet structures presented here reveal gross features in common with pleated sheets in amyloid fibrils. Rippled and pleated sheets both assemble on a cross- $\beta$  scaffold, producing fibrillar superstructures. Both types of sheets can mate together to form dry interfaces, the strength of which varies according to the amino acid sequence. The structures also reveal fundamental differences in the arrangement of side chains on sheet surfaces. Side chains on the rippled sheet surface are more loosely arranged compared to the pleated sheet (Figure 6), potentially enabling a greater range of rotameric freedom than that observed in pleated sheets. It is also worth noting that all five of the rippled sheets we observed here are antiparallel, whereas the overwhelming majority of amyloid fibrils adopt parallel in-register sheets. Could our lack of observation of parallel in-register rippled sheets be attributed to the incapability of rippled sheets to form stabilizing polar or aromatic ladders (Figure 6D) or is it merely an artifact of the sequence space examined here? Furthermore, can racemic mixtures of longer segments mimic the complex meandering folds and extraordinary thermodynamic stability of amyloid fibrils? Future exploration of the rippled sheet structural space will help answer these questions.

## CONCLUSIONS

We presented atomic resolution structures of five distinct rippled  $\beta$ -sheets. The structures described herein vary in terms of length and sequence complexity, incorporating charged,

polar, and hydrophobic residues. Our results reinforce the hypothesis that rippled sheet formation from racemic mixtures of aggregating peptides is preferred over homochiral self-assembly in three-dimensional systems. Moreover, in contrast to homochiral amyloid fibrils, the formation of a steric zipper is not a necessary condition for rippled  $\beta$ -sheet fibrils to form; changes in sequence and solvent can influence the architecture of the fibrils, leading to new structural motifs.

## ■ ASSOCIATED CONTENT

### § Supporting Information

The Supporting Information is available free of charge at <https://pubs.acs.org/doi/10.1021/jacs.3c11712>.

Crystallization protocols, structural refinement parameters and additional tables are provided free of charge; the rippled sheet structural files have been deposited at the PDB under reference numbers 8T89 (KLVFFA:klvffa); 8T84 (MVGGVV:mvgvvv, HF1P); 8T82 (MVGGVV:mvgvvv, PFFA), and 8T86 (AILSS:ailss) ([PDF](#))

## ■ AUTHOR INFORMATION

### Corresponding Authors

Amaruka Hazari — Dept. of Chemistry and Biochemistry,  
UCSC, Santa Cruz, California 95064, United States;  
Email: [amhazari@ucsc.edu](mailto:amhazari@ucsc.edu)

Jevgenij A. Raskatov — Dept. of Chemistry and Biochemistry,  
UCSC, Santa Cruz, California 95064, United States;  
[ORCID: 0000-0002-0082-9113](https://orcid.org/0000-0002-0082-9113); Email: [jraskato@ucsc.edu](mailto:jraskato@ucsc.edu)

### Authors

Michael R. Sawaya — Dept. of Chemistry and Biochemistry,  
UCLA, Los Angeles, California 90095-1569, United States;  
[ORCID: 0000-0003-0874-9043](https://orcid.org/0000-0003-0874-9043)

Maria Sajimon — Dept. of Chemistry and Biochemistry,  
UCSC, Santa Cruz, California 95064, United States;  
[ORCID: 0000-0002-6753-6841](https://orcid.org/0000-0002-6753-6841)

Niko Vlahakis — Dept. of Chemistry and Biochemistry, UCLA,  
Los Angeles, California 90095-1569, United States

Jose Rodriguez — Dept. of Chemistry and Biochemistry,  
UCLA, Los Angeles, California 90095-1569, United States

David Eisenberg — Dept. of Chemistry and Biochemistry,  
UCLA, Los Angeles, California 90095-1569, United States

Complete contact information is available at:  
<https://pubs.acs.org/10.1021/jacs.3c11712>

### Author Contributions

§ A.H. and M.R.S. contributed equally to this work.

### Notes

The authors declare no competing financial interest.

## ■ ACKNOWLEDGMENTS

Dedicated to Harry Barkus Gray; A.H. and J.A.R. thank the Seaver Institute for a generous gift. We acknowledge the NIH R01AG070895, R01AG048120, RF1AG065407, and R01AG074954. We thank the NSF (MCB1616265) and the California NanoSystems Institute at the University of California, Los Angeles. The authors also acknowledge the Department of Energy Grant DE-FC02-02ER63421 for support. This work is based upon research conducted at the Northeastern Collaborative Access Team beamline 24-ID-E,

which is funded by the National Institute of General Medical Sciences from the National Institutes of Health (P30 GM124165). The Eiger 16M detector is funded by a NIH-ORIP HEI grant (S10OD021527). This research used resources of the Advanced Photon Source, a U.S. Department of Energy (DOE) Office of Science User Facility operated for the DOE Office of Science by Argonne National Laboratory, under Contract No. DE-AC02-06CH11357. We thank Duilio Cascio for support during data collection and refinement.

## ■ REFERENCES

- (1) Raskatov, J. A.; Teplow, D. B. Using chirality to probe the conformational dynamics and assembly of intrinsically disordered amyloid proteins. *Sci. Rep.* **2017**, *7* (1), No. 12433.
- (2) Anil, B.; Song, B.; Tang, Y.; Raleigh, D. P. Exploiting the Right Side of the Ramachandran Plot: Substitution of Glycines by d-Alanine Can Significantly Increase Protein Stability. *J. Am. Chem. Soc.* **2004**, *126* (41), 13194–13195.
- (3) Culik, R. M.; Annavarapu, S.; Nanda, V.; Gai, F. Using D-amino acids to delineate the mechanism of protein folding: Application to Trp-cage. *Chem. Phys.* **2013**, *422*, 131–134.
- (4) Hua, Q.-X.; Nakagawa, S.; Hu, S.-Q.; Jia, W.; Wang, S.; Weiss, M. A. Toward the Active Conformation of Insulin: Stereospecific Modulation of a Structural Switch in the B Chain. *J. Biol. Chem.* **2006**, *281* (34), 24900–24909.
- (5) Dutta, S.; Foley, A. R.; Warner, C. J. A.; Zhang, X.; Rolandi, M.; Abrams, B.; Raskatov, J. A. Suppression of Oligomer Formation and Formation of Non-Toxic Fibrils upon Addition of Mirror-Image  $\text{A}\beta$ 42 to the Natural L-Enantiomer. *Angew. Chem., Int. Ed.* **2017**, *56* (38), 11506–11510.
- (6) Foley, A. R.; Finn, T. S.; Kung, T.; Hatami, A.; Lee, H.-W.; Jia, M.; Rolandi, M.; Raskatov, J. A. Trapping and Characterization of Nontoxic  $\text{A}\beta$ 42 Aggregation Intermediates. *ACS Chem. Neurosci.* **2019**, *10* (8), 3880–3887.
- (7) Foley, A. R.; Roseman, G. P.; Chan, K.; Smart, A.; Finn, T. S.; Yang, K.; Lokey, R. S.; Millhauser, G. L.; Raskatov, J. A. Evidence for aggregation-independent, PrP(C)-mediated  $\text{A}\beta$  cellular internalization. *Proc. Natl. Acad. Sci. U.S.A.* **2020**, *117* (46), 28625–28631.
- (8) Garcia, A. M.; Giorgiutti, C.; El Khoury, Y.; Bauer, V.; Spiegelhalter, C.; Leize-Wagner, E.; Hellwig, P.; Potier, N.; Torbeev, V. Aggregation and Amyloidogenicity of the Nuclear Coactivator Binding Domain of CREB-Binding Protein. *Chem. - Eur. J.* **2020**, *26* (44), 9889–9899.
- (9) Nagy, K. J.; Giano, M. C.; Jin, A.; Pochan, D. J.; Schneider, J. P. Enhanced Mechanical Rigidity of Hydrogels Formed from Enantiomeric Peptide Assemblies. *J. Am. Chem. Soc.* **2011**, *133* (38), 14975–14977.
- (10) Nagy-Smith, K.; Beltramo, P. J.; Moore, E.; Tycko, R.; Furst, E. M.; Schneider, J. P. Molecular, Local, and Network-Level Basis for the Enhanced Stiffness of Hydrogel Networks Formed from Coassembled Racemic Peptides: Predictions from Pauling and Corey. *ACS Cent. Sci.* **2017**, *3* (6), 586–597.
- (11) Swanekamp, R. J.; DiMaio, J. T. M.; Bowerman, C. J.; Nilsson, B. L. Coassembly of Enantiomeric Amphipathic Peptides into Amyloid-Inspired Rippled  $\beta$ -Sheet Fibrils. *J. Am. Chem. Soc.* **2012**, *134* (12), 5556–5559.
- (12) Swanekamp, R. J.; Welch, J. J.; Nilsson, B. L. Proteolytic stability of amphipathic peptide hydrogels composed of self-assembled pleated  $\beta$ -sheet or coassembled rippled  $\beta$ -sheet fibrils. *Chem. Commun.* **2014**, *50* (70), 10133–10136.
- (13) Urban, J. M.; Ho, J.; Piester, G.; Fu, R.; Nilsson, B. L. Rippled  $\beta$ -Sheet Formation by an Amyloid- $\beta$  Fragment Indicates Expanded Scope of Sequence Space for Enantiomeric  $\beta$ -Sheet Peptide Coassembly. *Molecules* **2019**, *24*, No. 1983, DOI: 10.3390/molecules24101983.
- (14) Wong, K. M.; Robang, A. S.; Lint, A. H.; Wang, Y.; Dong, X.; Xiao, X.; Seroski, D. T.; Liu, R.; Shao, Q.; Hudalla, G. A.; et al.

- Engineering  $\beta$ -Sheet Peptide Coassemblies for Biomaterial Applications. *J. Phys. Chem. B* **2021**, *125* (50), 13599–13609.
- (15) Pauling, L.; Corey, R. B. Two Rippled-Sheet Configurations of Polypeptide Chains, and a Note about the Pleated Sheets. *Proc. Natl. Acad. Sci. U.S.A.* **1953**, *39* (4), 253–256.
- (16) Colonna-Cesarri, F.; Premilat, S.; Lotz, B. Structure of polyglycine I: A comparison of the antiparallel pleated and antiparallel rippled sheets. *J. Mol. Biol.* **1974**, *87* (2), 181–191.
- (17) Lotz, B. Rippled Sheets: The Early Polyglycine Days and Recent Developments in Nylons. *ChemBioChem* **2022**, *23* (5), No. e202100658.
- (18) Moore, W. H.; Krimm, S. Vibrational analysis of peptides, polypeptides, and proteins. I. Polyglycine I. *Biopolymers* **1976**, *15* (12), 2439–2464.
- (19) Fuhrhop, J.-H.; Krull, M.; Büldt, G. Precipitates with  $\beta$ -Pleated Sheet Structure by Mixing Aqueous Solutions of Helical Poly(D-lysine) and Poly(L-lysine). *Angew. Chem., Int. Ed.* **1987**, *26* (7), 699–700.
- (20) Weissbuch, I.; Illos, R. A.; Bolbach, G.; Lahav, M. Racemic  $\beta$ -Sheets as Templates of Relevance to the Origin of Homochirality of Peptides: Lessons from Crystal Chemistry. *Acc. Chem. Res.* **2009**, *42* (8), 1128–1140.
- (21) Dutta, S.; Finn, T. S.; Kuhn, A. J.; Abrams, B.; Raskatov, J. A. Chirality Dependence of Amyloid  $\beta$  Cellular Uptake and a New Mechanistic Perspective. *ChemBioChem* **2019**, *20* (8), 1023–1026.
- (22) Hazari, A.; Sawaya, M. R.; Vlahakis, N.; Johnstone, T. C.; Boyer, D.; Rodriguez, J.; Eisenberg, D.; Raskatov, J. A. The rippled  $\beta$ -sheet layer configuration—a novel supramolecular architecture based on predictions by Pauling and Corey. *Chem. Sci.* **2022**, *13* (31), 8947–8952.
- (23) Kuhn, A. J.; Ehlke, B.; Johnstone, T. C.; Oliver, S. R. J.; Raskatov, J. A. A crystal-structural study of Pauling–Corey rippled sheets. *Chem. Sci.* **2022**, *13* (3), 671–680.
- (24) Raskatov, J. A.; Foley, A. R.; Louis, J. M.; Yau, W.-M.; Tycko, R. Constraints on the Structure of Fibrils Formed by a Racemic Mixture of Amyloid- $\beta$  Peptides from Solid-State NMR, Electron Microscopy, and Theory. *J. Am. Chem. Soc.* **2021**, *143* (33), 13299–13313.
- (25) Raskatov, J. A.; Schneider, J. P.; Nilsson, B. L. Defining the Landscape of the Pauling–Corey Rippled Sheet: An Orphaned Motif Finding New Homes. *Acc. Chem. Res.* **2021**, *54* (10), 2488–2501.
- (26) Grellich-Mucha, M.; Garcia, A. M.; Torbeev, V.; Ożga, K.; Berlicki, Ł.; Olesiak-Bańska, J. Autofluorescence of Amyloids Determined by Enantiomeric Composition of Peptides. *J. Phys. Chem. B* **2021**, *125* (21), 5502–5510.
- (27) Li, X.; Rios, S. E.; Nowick, J. S. Enantiomeric  $\beta$ -sheet peptides from  $\text{A}\beta$  form homochiral pleated  $\beta$ -sheets rather than heterochiral rippled  $\beta$ -sheets. *Chem. Sci.* **2022**, *13* (26), 7739–7746.
- (28) Sawaya, M. R.; Sambashivan, S.; Nelson, R.; Ivanova, M. I.; Sievers, S. A.; Apostol, M. I.; Thompson, M. J.; Balbirnie, M.; Wiltzius, J. J. W.; McFarlane, H. T.; et al. Atomic structures of amyloid cross- $\beta$  spines reveal varied steric zippers. *Nature* **2007**, *447* (7143), 453–457.
- (29) Wallach, O. Zur Kenntnis der Terpene und der ätherischen Öle. *Justus Liebigs Ann. Chem.* **1895**, *286*, 90–143, DOI: [10.1002/jlac.18952860105](https://doi.org/10.1002/jlac.18952860105).
- (30) Dunitz, J. D.; Gavezzotti, A. Proteogenic Amino Acids: Chiral and Racemic Crystal Packings and Stabilities. *J. Phys. Chem. B* **2012**, *116* (23), 6740–6750.
- (31) Zee, C.-T.; Glynn, C.; Gallagher-Jones, M.; Miao, J.; Santiago, C. G.; Cascio, D.; Gonen, T.; Sawaya, M. R.; Rodriguez, J. A. Homochiral and racemic MicroED structures of a peptide repeat from the ice-nucleation protein InaZ. *IUCrJ* **2019**, *6* (2), 197–205.
- (32) Liu, X.; Gellman, S. H. Comparisons of  $\beta$ -Hairpin Propensity Among Peptides with Homochiral or Heterochiral Strands. *ChemBioChem* **2021**, *22* (18), 2772–2776.
- (33) Chung, D. M.; Nowick, J. S. Enantioselective Molecular Recognition between  $\beta$ -Sheets. *J. Am. Chem. Soc.* **2004**, *126* (10), 3062–3063.
- (34) Eisenberg, D. S.; Sawaya, M. R. Structural Studies of Amyloid Proteins at the Molecular Level. *Annu. Rev. Biochem.* **2017**, *86* (1), 69–95.
- (35) Balbirnie, M.; Grothe, R.; Eisenberg, D. S. An amyloid-forming peptide from the yeast prion Sup35 reveals a dehydrated beta-sheet structure for amyloid. *Proc. Natl. Acad. Sci. U.S.A.* **2001**, *98* (5), 2375–2380.
- (36) von Bergen, M.; Friedhoff, P.; Biernat, J.; Heberle, J.; Mandelkow, E. M.; Mandelkow, E. Assembly of tau protein into Alzheimer paired helical filaments depends on a local sequence motif ( $^{306}\text{VQIVYK}^{311}$ ) forming beta structure. *Proc. Natl. Acad. Sci. U.S.A.* **2000**, *97* (10), 5129–5134.
- (37) von Bergen, M.; Barghorn, S.; Li, L.; Marx, A.; Biernat, J.; Mandelkow, E. M.; Mandelkow, E. Mutations of tau protein in frontotemporal dementia promote aggregation of paired helical filaments by enhancing local beta-structure. *J. Biol. Chem.* **2001**, *276* (51), 48165–48174.
- (38) Ivanova, M. I.; Sievers, S. A.; Sawaya, M. R.; Wall, J. S.; Eisenberg, D. Molecular basis for insulin fibril assembly. *Proc. Natl. Acad. Sci. U.S.A.* **2009**, *106* (45), 18990–18995.
- (39) Moriarty, D. F.; Raleigh, D. P. Effects of sequential proline substitutions on amyloid formation by human amylin $20\text{--}29$ . *Biochemistry* **1999**, *38* (6), 1811–1818.
- (40) Lawrence, M. C.; Colman, P. M. Shape complementarity at protein/protein interfaces. *J. Mol. Biol.* **1993**, *234* (4), 946–950.

CAS BIOFINDER DISCOVERY PLATFORM™

**PRECISION DATA  
FOR FASTER  
DRUG  
DISCOVERY**

CAS BioFinder helps you identify targets, biomarkers, and pathways

**Unlock insights**

**CAS**  
A division of the  
American Chemical Society